High resolution direct measurement of temperature distribution in silicon nanophotonics devices

Mor Tzur, Boris Desiatov, Ilya Goykhman, Meir Grajower, and Uriel Levy*

Department of Applied Physics, The Benin School of Engineering and Computer Science, The Center for Nanoscience and Nanotechnology, The Hebrew University of Jerusalem, Jerusalem, 91904, Israel
ulevy@mail.huji.ac.il

Abstract: Following the miniaturization of photonic devices and the increase in data rates, the issues of self heating and heat removal in active nanophotonic devices should be considered and studied in more details. In this paper we use the approach of Scanning Thermal Microscopy (SThM) to obtain an image of the temperature field of a silicon micro ring resonator with sub-micron spatial resolution. The temperature rise in the device is a result of self heating which is caused by free carrier absorption in the doped silicon. The temperature is measured locally and directly using a temperature sensitive AFM probe. We show that this local temperature measurement is feasible in the photonic device despite the perturbation that is introduced by the probe. Using the above method we observed a significant self heating of about 10 degrees within the device.

©2013 Optical Society of America

OCIS codes: (180.4243) Near-field microscopy; (230.5750) Resonators.

References and links

1. Y. Joshi and P. Kumar, *Energy Efficient Thermal Management of Data Centers* (Springer, 2012).
2. M. Paniccia, "Integrating silicon photonics," Nat. Photonics **4**(8), 498–499 (2010).
3. D. A. B. Miller, "Optical interconnects to electronic chips," Appl. Opt. **49**(25), F59–F70 (2010).
4. P. Pepeljugoski, J. Kash, F. Doany, D. Kuchta, L. Schares, C. Schow, M. Taubenblatt, B. J. Offrein, and A. Benner, "Low power and high density optical interconnects for future supercomputers," in Optical Fiber Communication Conference (OFC2010), paper OThX2.
5. E. Ozbay, "Plasmonics: merging photonics and electronics at nanoscale dimensions," Science **311**(5758), 189–193 (2006).
6. J. A. Conway, S. Sahni, and T. Szkopek, "Plasmonic interconnects versus conventional interconnects: a comparison of latency, crosstalk and energy costs," Opt. Express **15**(8), 4474–4484 (2007).
7. J. A. Schuller, E. S. Barnard, W. Cai, Y. C. Jun, J. S. White, and M. L. Brongersma, "Plasmonics for extreme light concentration and manipulation," Nat. Mater. **9**(3), 193–204 (2010).
8. V. J. Sorger, N. D. Lanzillotti-Kimura, R. Ma, and X. Zhang, "Ultra-compact silicon nanophotonic modulator with broadband response," J. Nanophotonics **1**, 17–22 (2012).
9. M. W. Knight, H. Sobhani, P. Nordlander, and N. J. Halas, "Photodetection with active optical antennas," Science **332**(6030), 702–704 (2011).
10. S. Li, N. G. Tarr, and P. Berini, "Schottky photodetector integration on LOCOS-defined SOI waveguides," Proc. SPIE **7750**, 77501M (2010).
11. I. Goykhman, B. Desiatov, J. Khurgin, J. Shappir, and U. Levy, "Locally oxidized silicon Surface-Plasmon schottky detector for telecom regime," Nano Lett. **11**(6), 2219–2224 (2011).
12. S. Zhu, M. B. Yu, G. Q. Lo, and D. L. Kwong, "Near-infrared waveguide-based nickel silicide schottky-barrier photodetector for optical communications," Appl. Phys. Lett. **92**(8), 081103 (2008).
13. D. Cahill, K. Goodson, and A. Majumdar, "Thermometry and thermal transport in micro/nanoscale solid-state devices and structures," J. Heat Transfer **124**(2), 223–241 (2002).
14. D. G. Cahill, W. K. Ford, K. E. Goodson, G. D. Mahan, A. Majumdar, H. J. Maris, R. Merlin, and S. R. Phillpot, "Nanoscale thermal transport," J. Appl. Phys. **93**(2), 793–818 (2003).
15. L. Shi and A. Majumdar, "Thermal transport mechanisms at nanoscale point contacts," J. Heat Transfer **124**(2), 329–337 (2002).
16. S. Sadat, A. Tan, Y. J. Chua, and P. Reddy, "Nanoscale thermometry using point contact thermocouples," Nano Lett. **10**(7), 2613–2617 (2010).
17. G. Wielgoszewski, P. Sulecki, P. Janus, P. Grabiec, E. Zschech, and T. Gotszalk, "A high-resolution measurement system for novel scanning thermal microscopy resistive nanoprobes," Meas. Sci. Technol. **22**(9), 094023 (2011).

#197482 - $15.00 USD Received 10 Sep 2013; revised 3 Nov 2013; accepted 5 Nov 2013; published 18 Nov 2013

18. M. E. McConney, D. D. Kulkarni, H. Jiang, T. J. Bunning, and V. V. Tsukruk, "A new twist on scanning thermal microscopy," Nano Lett. **12**(3), 1218–1223 (2012).
19. K. Kim, W. Jeong, W. Lee, and P. Reddy, "Ultra-High vacuum scanning thermal microscopy for nanometer resolution quantitative thermometry," ACS Nano **6**(5), 4248–4257 (2012).
20. K. Kim, J. Chung, G. Hwang, O. Kwon, and J. S. Lee, "Quantitative measurement with scanning thermal microscope by preventing the distortion due to the heat transfer through the air," ACS Nano **5**(11), 8700–8709 (2011).
21. X. Zheng, J. Lexau, Y. Luo, H. Thacker, T. Pinguet, A. Mekis, G. Li, J. Shi, P. Amberg, N. Pinckney, K. Raj, R. Ho, J. E. Cunningham, and A. V. Krishnamoorthy, "Ultra-low-energy all-CMOS modulator integrated with driver," Opt. Express **18**(3), 3059–3070 (2010).
22. D. J. Thomson, F. Y. Gardes, G. T. Reed, F. Milesi, and J.-M. Fédéli, "High speed silicon optical modulator with self aligned fabrication process," Opt. Express **18**(18), 19064–19069 (2010).
23. Q. Xu, B. Schmidt, S. Pradhan, and M. Lipson, "Micrometre-scale silicon electro-optic modulator," Nature **435**(7040), 325–327 (2005).
24. A. Liu, L. Liao, Y. Chetrit, J. Basak, H. Nguyen, D. Rubin, and M. Paniccia, "Wavelength Division Multiplexing Based Photonic Integrated Circuits on Silicon-on-Insulator Platform," IEEE J. Sel. Top. Quantum Electron. **16**(1), 23–32 (2010).
25. J. W. Park, J.-B. You, I. G. Kim, and G. Kim, "High-modulation efficiency silicon Mach-Zehnder optical modulator based on carrier depletion in a PN Diode," Opt. Express **17**(18), 15520–15524 (2009).
26. T. Tanabe, K. Nishiguchi, E. Kuramochi, and M. Notomi, "Low power and fast electro-optic silicon modulator with lateral p-i-n embedded photonic crystal nanocavity," Opt. Express **17**(25), 22505–22513 (2009).
27. R. Soref and B. Bennett, "Electrooptical effects in silicon," IEEE J. Quantum Electron. **23**(1), 123–129 (1987).
28. J. E. Heebner, R. Grover, and T. Ibrahim, *Optical Microresonators: Theory, Fabrication, and Applications* (Springer, 2008).
29. M. Abashin, U. Levy, K. Ikeda, and Y. Fainman, "Effects produced by metal-coated near-field probes on the performance of silicon waveguides and resonators," Opt. Lett. **32**(17), 2602–2604 (2007).
30. B. Guha, C. Otey, C. B. Poitras, S. Fan, and M. Lipson, "Near-Field radiative cooling of nanostructures," Nano Lett. **12**(9), 4546–4550 (2012).
31. M. C. Salvadori, A. R. Vaz, F. S. Teixeira, M. Cattani, and I. G. Brown, "Thermoelectric effect in very thin film Pt/Au thermocouples," Appl. Phys. Lett. **88**(13), 133106 (2006).
32. G. Ghosh, *Handbook of Thermo-Optic Coefficients of Optical Materials with Applications* (Academic, 1998).
33. X. Zheng, Y. Luo, G. Li, I. Shubin, H. Thacker, J. Yao, K. Raj, J. E. Cunningham, and A. V. Krishnamoorthy, "Enhanced optical bistability from self-heating due to free carrier absorption in substrate removed silicon ring modulators," Opt. Express **20**(10), 11478–11486 (2012).
34. M. R. Watts, W. A. Zortman, D. C. Trotter, G. N. Nielson, D. L. Luck, and R. W. Young, "Adiabatic Resonant Microrings (ARMs) with Directly Integrated Thermal Microphotonics," in Conference on Lasers and Electro-Optics/International Quantum Electronics Conference, p. CPDB10 (2009).
35. L. W. Luo, G. S. Wiederhecker, K. Preston, and M. Lipson, "Power insensitive silicon microring resonators," Opt. Lett. **37**(4), 590–592 (2012).
36. Y. Vlasov, W. M. J. Green, and F. Xia, "High-throughput silicon nanophotonic wavelength-insensitive switch for on-chip optical networks," Nat. Photonics **2**(4), 242–246 (2008).

1. Introduction

With the ever increased density of transistors on a chip and the higher operation rates, the power densities of typical integrated circuits are approaching the value of ~10W/cm^2 [1], comparable to a light bulb filament. Self heating and heat removal are becoming the limiting factor preventing further improvement in chip scale electronic circuits. Seeking for alternative technologies, on chip optical communication seems to be an attractive choice, giving rise to the field of silicon photonics [2–4] and very recently also to plasmonic interconnects [5–7]. However, photonic components, and in particular active components are also not free from self heating. Following the reduction in feature size of active photonic and plasmonic components towards the nanoscale [8–12], self-heating in such components may become a significant issue owing to the increasing optical power densities and the significant light absorption in the materials. Therefore, similar to electronics, nanoscale thermal characterization of photonic devices is important for understanding the underlying physics of self heating at the nanoscale, as well as for the development of advance on chip photonic components and circuits. Indeed, being able to directly measure the temperature of integrated photonic devices at the nanoscale may pave the way for developing approaches for controlling heat dissipation, designing thermally stable devices and enable their dense integration on chip.

In recent years, several approaches were developed in order to obtain thermal information with sub-micron spatial resolution [13,14], among them Scanning Thermal Microscopy

#197482 - $15.00 USD Received 10 Sep 2013; revised 3 Nov 2013; accepted 5 Nov 2013; published 18 Nov 2013
(C) 2013 OSA

(SThM). SThM is an AFM-based technique which utilizes temperature sensitive probe in order to scan a sample surface and generate a mapping of the temperature field. Different sensing probes were designed and investigated, including thermocouples [15,16], thermo-resistive [17] and bimorphs [18]. Many of these configurations provide a temperature sensor which is independent of the measured sample, and capable of measuring any combination of dielectric or metallic substances. This property is highly useful for the investigation of photonic and plasmonic devices. Being intensively developed, SThM was shown to obtain temperature profiles with spatial resolution of ~10nm and excellent thermal resolution of ~15mK [19]. Recently it also showed great progress towards accurate quantitative measurement of the local temperature by developing a procedure which removes the effect of the tip heating via the air [20].

In this paper we use SThM experimental scheme to demonstrate a direct measurement of the temperature distribution of silicon photonic chip using a thermocouple probe. Specifically, we focus on the thermal properties of a doped micro ring resonator, of the same type which has been demonstrated for active photonics applications such as photonic modulators [21,22]. The temperature mapping of the system is recorded when the ring is at resonance and out of resonance. The results indicate a significant self heating which must be taken into account. Furthermore, the important question of the perturbation of the tip influencing the measured results is addressed. As will shown, naïvely neglecting this effect in systems operating at resonance is far from being sufficient.

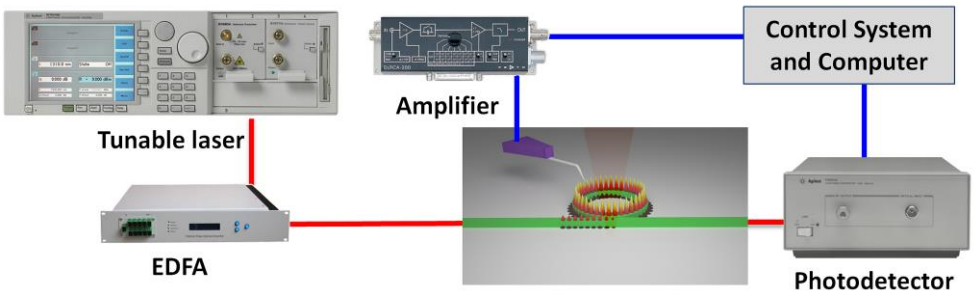

Fig. 1. Schematic representation of the experimental setup for the simultaneous thermal and optical transmission measurement.

2. Experiments

To demonstrate a nanophotonic device self-heating we have constructed the experimental setup depicted in Fig. 1. A TE polarized light derived from a tunable laser (Agilent 81680A) operating around 1550nm wavelength was coupled into the tapered ends of the chip waveguides using polarization maintaining lensed fibers. The device was not optimized for minimal insertion loss (estimated loss is about 15dB per facet). The laser signal was amplified using erbium doped fiber amplifier (EDFA, RED-C) and the output light was detected by an InGaAs photodetector (HP 81634B). As mentioned before, our device of choice was a Micro Ring Resonator (MRR) with a single bus waveguide coupled to the ring. The ring radius is 6μm and the gap in the coupling region is 200nm.The device was fabricated on a silicon-on-insulator substrate with 2μm oxide layer below separating between the waveguide structure and the silicon substrate. The waveguides width was set to 450nm and their height was 250nm including a 20nm silicon rib as shown schematically in Fig. 2(c). In Fig. 2(a) a Scanning Electron Micrograph (SEM) of the fabricated microring is shown. The temperature measurement was done using thermocouple probes purchased from Nanonics and mounted on a Nanonics MultiView-4000 head. The probes consist of a Pt wire running through a metal-coated glass nano-pipette and slightly protruding over its edge. The external Au coating

#197482 - $15.00 USD Received 10 Sep 2013; revised 3 Nov 2013; accepted 5 Nov 2013; published 18 Nov 2013
(C) 2013 OSA

extends over the Pt wire, forming the thermocouple junction between the two metals. Typical tip diameter at the apex is 150-300nm. The thermocouple probe was connected to the control system through a low-noise trans impedance amplifier (FEMTO DLPCA-200).

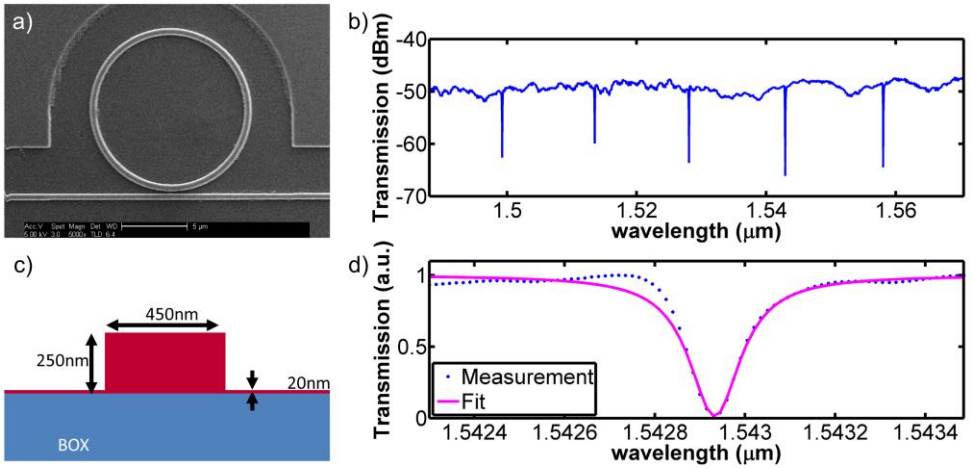

Fig. 2. (a) Top view SEM image of the measured silicon micro ring resonator (b) Measured transmission spectrum of the device (c) Schematic cross section diagram of the silicon waveguide (d) Lorentzian fit to a single resonance dip used for obtaining the resonator's quality factor.

3. Results and discussion

First, the transmission spectrum of the device was measured by scanning the tunable laser and collecting the data in the detector. The results in Figs. 2(b) and 2(d) show nice resonance dips with quality factor and finesse of Q≈11000 and F≈110, respectively.

Next, we turn into measuring the effect of self heating. The structure is Boron-doped with concentration level of $N = 5\cdot10^{17}$ atoms/cm^3, which is comparable to typical doping concentrations of active silicon photonic devices [22–26]. For such doping concentration, the self heating of the device is originated primarily from free carrier absorption (FCA). When 1550nm wavelength light is propagating in the waveguide, a portion of it is absorbed and dissipated as heat. The absorption coefficient was calculated using Soref empirical formula [27] $\alpha_{FC} = (8.5\cdot N_e + 6.0\cdot N_h)\cdot10^{-18}$ to be 3cm^{-1}. The effect of self heating is enhanced when the wavelength of light is tuned to one of the resonant wavelengths of the MRR due to the intensity buildup inside the resonator. The intensity buildup inside the resonator was calculated to be $I_{Ring} = 50\cdot I_{in}$ [28] and the power loss to heat is $P_{Heat} = 0.01\cdot P_{Light}$, where P_{Light} is the optical power inside the resonator.

To observe the effect of self heating, the laser wavelength was tuned to one of the MRR resonances. A thermocouple tip (200 nm in diameter) was placed in close proximity to the structure and a raster scan was executed. As a control experiment we repeated this measurement when the wavelength was detuned to 3nm away from the MRR resonance and also when the laser was turned off. The results are shown in Figs. 3(a)–3(f). It is apparent from Fig. 3(a) that when the laser is tuned to the MRR resonance there is a substantial rise in the thermal signal within the ring. Interestingly, maximum signal is obtained around the edges of the MRR waveguide. This is shown very clearly by taking a cross section across the waveguide of the MRR in Fig. 3(d). The reason for this interesting finding is related to the perturbation of the tip, as explained in more details in one of the subsequent sections. When the wavelength is tuned to be out of resonance, see Fig. 3(b), the rise in thermal signal is only marginal (shown by the corresponding cross section in Fig. 3(d)). The slight increase may be explained by the small on-resonance contribution of the amplified spontaneous emission (ASE) coming from the EDFA. This can be eliminated by the use of a band pass filter. In

#197482 - $15.00 USD Received 10 Sep 2013; revised 3 Nov 2013; accepted 5 Nov 2013; published 18 Nov 2013
(C) 2013 OSA

addition, we extracted from Figs. 3(a) and 3(b) cross sections of the thermal signal along the bus waveguide as shown in Fig. 3(e). The result indicates that the temperature along the waveguide is approximately flat in case that the system is out of resonance. In case that the system is in resonance, the thermal signal undergoes a sudden drop at the coupling region and then stabilizes at a lower level. This is because the light is coupled into the ring and experiences a significant loss, such that only a small portion of the input signal is coupled back into the waveguide. A dark measurement (without the presence of an optical signal) serves as a control measurement, indicating that the electronic cross-talk in the system (cross talk between the error channel of the AFM and the signal channel) is small, as presented in Fig. 3(c).

Finally, we repeated the experiment with a similar un-doped device as shown in Fig. 3(f). For that purpose we selected a silicon MRR with identical geometrical dimensions and with very similar parameters (Q≈14000, F≈140). In this device we expect the losses to arise mostly as a result of scattering from bends and defects in the structure, with very little absorption. Thus heat generation is expected to be small. Thermal scans were executed with identical scan parameters and with similar optical intensity propagating in the waveguide, when the system was kept in-resonance and out-of-resonance. As expected, no traces of temperature rise were observed near the ring or over the bus waveguide in neither of the cases within the precision limits of our system.

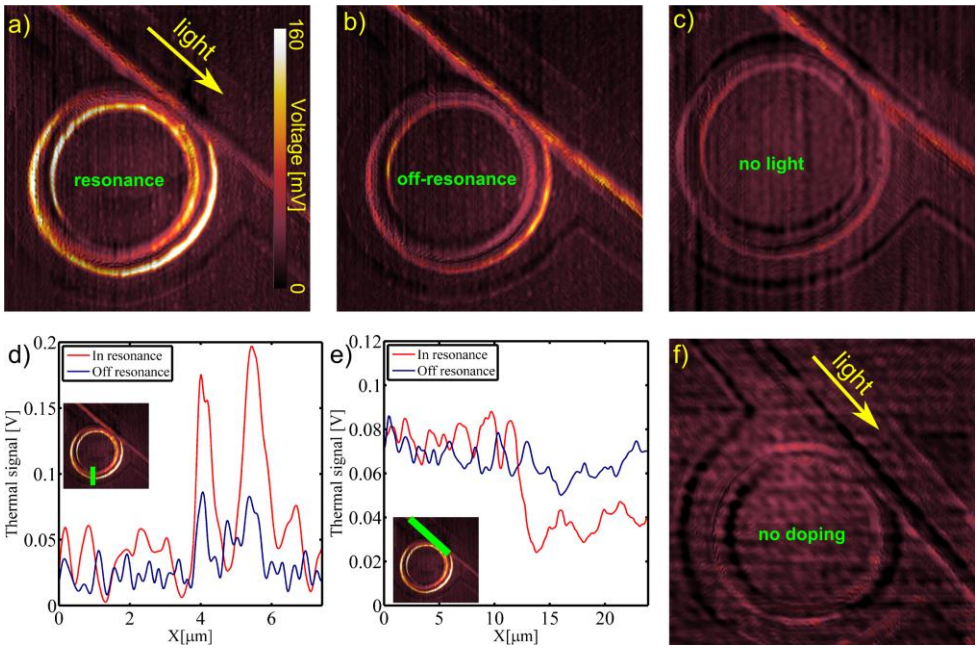

Fig. 3. Thermal images of the doped silicon MRR (a) in-resonance (b) out-of-resonance and (c) with no optical signal (laser turned off). (d) Cross section of the thermal signal over the ring waveguide (e) Cross section of the thermal signal along the bus waveguide. The cross section direction is shown in the inset. (f) A thermal image of the un-doped silicon MRR in resonance. The green wide lines in Figs. 3(d) and 3(e) show the location of the cross section in the image.

Next, we measured the temperature rise in the doped device while gradually increasing the input optical power. In Figs. 4(a)–4(c) we present thermal scans of doped MRR with increasing input optical power. In Fig. 4(d) we show that the temperature rise in the MRR is linear with the input power. This behavior is in agreement with the linear absorption mechanism resulting from FCA in the doped sample.

#197482 - $15.00 USD Received 10 Sep 2013; revised 3 Nov 2013; accepted 5 Nov 2013; published 18 Nov 2013
(C) 2013 OSA

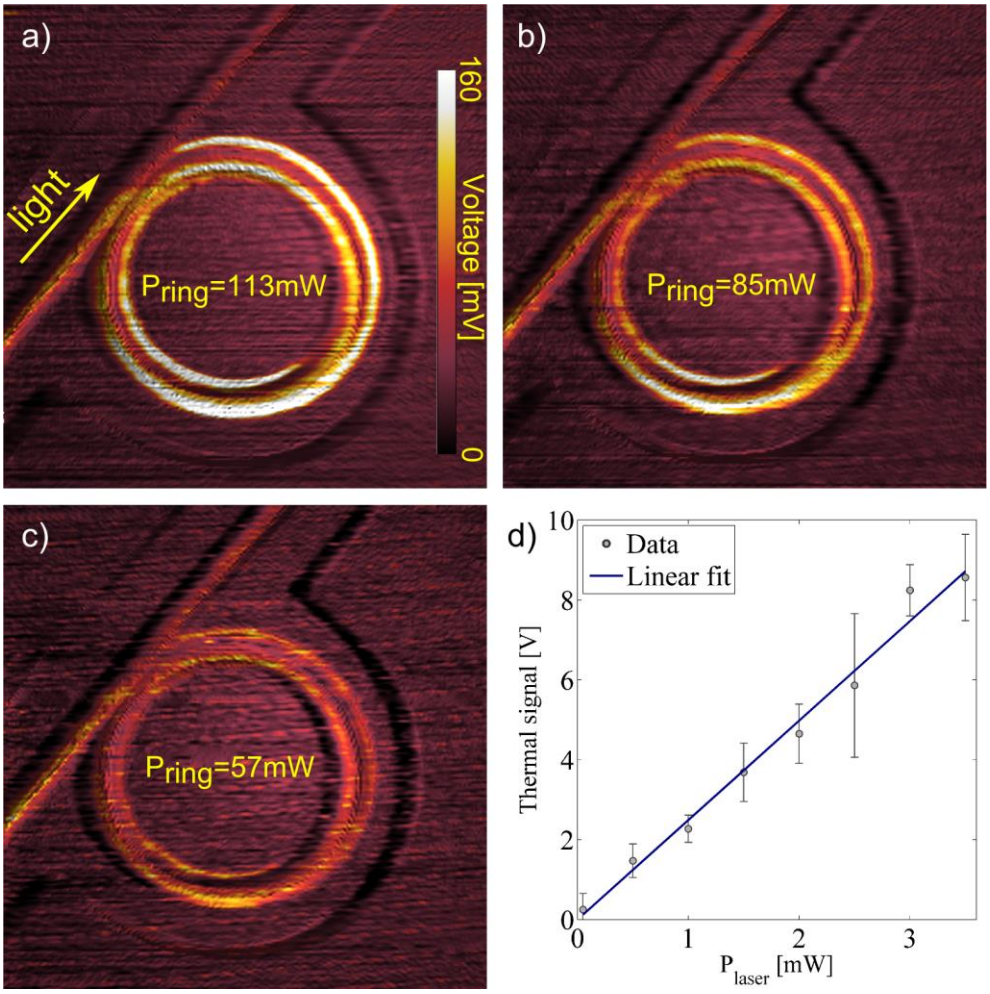

Fig. 4. Images (a)-(c) show thermal scans of the doped silicon MRR with increasing input optical power. P_{ring}, the optical power inside the ring, was calculated from the resonator's buildup factor and is indicated in each scan. (d) Linear fit for the thermal signal as a function of the change in the input optical power. Error bar was calculated from the difference between several thermal measurements.

The previous results indicate a clear self heating effect in the doped silicon sample. While the effect is clearly there, one needs to quantify the amount of temperature rise in order to be able to evaluate the effect of self heating on the performance of active silicon photonic devices. In the coming section we evaluate the effect of self heating in more details, taking into account effect of tip perturbation and also tip response to temperature rise in nanometric structures.

Naively, one may expect that the system remains in steady state during the scan. Therefore, one would expect a step-like temperature profile across the MRR waveguide. This expectation is practically contradicted by the sharp rise pattern near the edges of the MRR waveguide. The observed pattern can be explained using an optical transmission measurement taken at the through port of the MRR simultaneously with the thermal measurement. Figures 5(a)–5(c) present the topography, optical transmission and thermal images obtained by scanning the probe over the sample, respectively. The optical transmission image was captured by measuring the transmission of light through the output of the MRR as a function of the position of the thermal probe. Figure 5(d) shows a cross section of Figs. 5(a)–5(c) along the blue line, i.e. a cross section of the topography (blue), transmission (green) and

#197482 - $15.00 USD Received 10 Sep 2013; revised 3 Nov 2013; accepted 5 Nov 2013; published 18 Nov 2013
(C) 2013 OSA

topography (red). This result clearly shows that for a case where the wavelength is tuned to one of the MRR resonances, the transmission signal increases as tip approaches the MRR waveguide. i.e. the tip perturbs the optical signal. The effect of tip perturbation is well known and investigated and was already studied in the context of near-field photonic measurements [29]. The perturbation of the metal-coated tip is two-fold: first, it introduces high losses and therefore, the MRR is no longer around critical coupling condition. Second, the presence of the tip shifts the resonance wavelength of the MRR which is no longer matched to the wavelength of the laser. These two effects result in higher transmission through the bus waveguide. In fact, the effect is so strong such that the transmission value when the tip is located over the center of the MRR waveguide is very close to the transmission value in out-of-resonance state. The cross section of the thermal signal in Fig. 5(d) suggests that when the tip is placed at the center of the MRR waveguide, the MRR is no longer hot, probably because there is no longer resonant enhancement effect. In fact, there is an optimal distance between the tip and the MRR waveguide, for which the tip senses the temperature rise in the device while minimally affecting its performance. This is the reason for observing two spikes at the edges of the waveguide rather than a flat temperature profile.

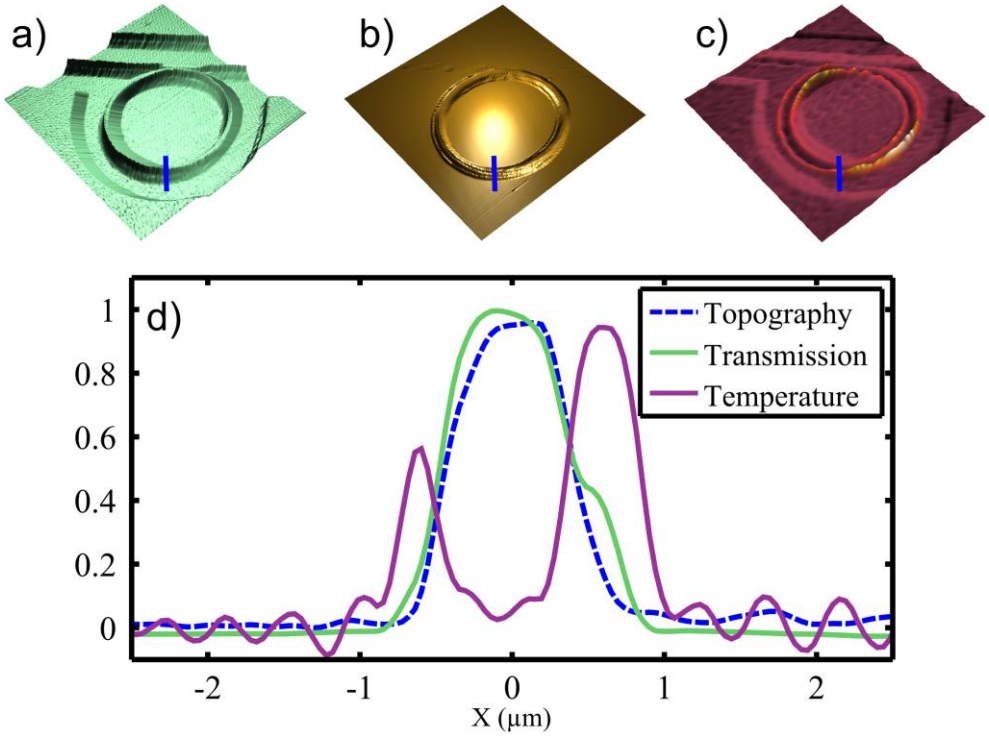

Fig. 5. (a) Topography, (b) optical transmission and (c) thermal images taken from a single scan. The blue lines in each of these panels represent the cross section which is shown in (d). The perturbation of the tip to the resonance is apparent from the change in optical transmission which closely follows the topography profile. The decrease in temperature is inversely correlated to the perturbation of the tip.

After gaining better understanding with regard to the two lobe thermal profile, we next turn into estimating the value of temperature rise. To do so, the measurement must be calibrated against a sample at known temperature. Previous works which thoroughly investigated thermocouple-based SThM measurement schemes indicated that close to room temperature, where conduction is the predominant heat transfer mechanism there exists a linear relation between the measured temperature rise and the real temperature rise in the sample [13, 15, 20]. At higher temperatures, radiative transfer between the sample and the tip

#197482 - $15.00 USD Received 10 Sep 2013; revised 3 Nov 2013; accepted 5 Nov 2013; published 18 Nov 2013
(C) 2013 OSA

can become a significant mechanism as recently shown by Lipson et al [30]. The temperature differences discussed in this paper are on the scale of up to 10 degrees, and thus we do not take the mechanism of radiation into account. The proportion coefficient between the measured and the actual temperature theoretically depends on the thermal resistance values of the different components of the system's thermal circuit. However, it was also shown [15] that this coefficient does change in a non-linear fashion as the measured feature size decreases. Therefore, the calibration coefficient for our measurement ($f_{Calibration}$, representing the system temperature response for a certain feature size) may be extracted from a measurement of a controlled sample with similar characteristic width. For this purpose we used a set of thin film Au resistors in different widths. The resistors were joule-heated to a set of known temperatures, previously determined using a 4-probe resistivity measurements combined with temperature coefficient of resistance (TCR) measurement. The temperature of the resistors was then measured using an identical scan setup and was compared to the real temperature. The calibration coefficient for a feature with 450nm width was found to be 0.22 ± 0.02. The calibration coefficients ranged between 0.16 and 0.4 for width values range of 400nm-1000nm respectively. The calibration relation was therefore: $\Delta T_{Meausred} = f_{Calibration} \cdot \Delta T_{Real}$. The measured voltage was translated to temperature using $\Delta V_{Junction} = S_{Pt-Au} \cdot \Delta T_{Meausred}$ and the parameters of the accompanied electric circuit $\Delta V_{Measured} = G \cdot \Delta V_{Junction} / R$ where G and R are the amplification factor of the low-noise amplifier and the junction resistance, respectively. Due to the relatively large dimensions of the thermocouple junction, we assume size effects to be negligible in our case and thus we use the bulk value for the junction thermopower $S_{Pt-Au} = 6.5\mu V/K$ [31].

Figure 6(a) shows a 1D cross section of the temperature rise over the ring waveguide for Fig. 6(b). The measurement results are shown before and after calibration (dashed black line and solid blue line, respectively). The maximal and average temperature difference along the ring edges after calibration was found to be 9.8K and 3.3 ± 0.4K respectively. The average temperature difference was obtained using averaging the thermal signal over the circumference of the inner and outer edges of the ring.

Figure 6(a) also presents simulation results for the given conditions. The temperature distribution Fig. 6(c) and the optical power Fig. 6(d) in the ring was simulated using finite element method software (COMSOL). First, we calculated the temperature distribution in a cross section of the ring waveguide for a constant optical intensity inside the ring (dashed red line). Then, we used the optical transmission measurement in order to extract the loss which is introduced by the tip at each position. This enabled us to calculate the buildup factor, and thus the optical power in the ring, as a function of the tip position along the cross section. This results with two spikes temperature profile (solid red line) similar to the profile observed by the measurement. While this approach shows encouraging results qualitatively predicting the tip effect on the temperature profile, further investigation of the thermal properties of the system is needed in order to develop a model which is capable of supplying accurate quantitative predictions.

#197482 - $15.00 USD Received 10 Sep 2013; revised 3 Nov 2013; accepted 5 Nov 2013; published 18 Nov 2013
(C) 2013 OSA

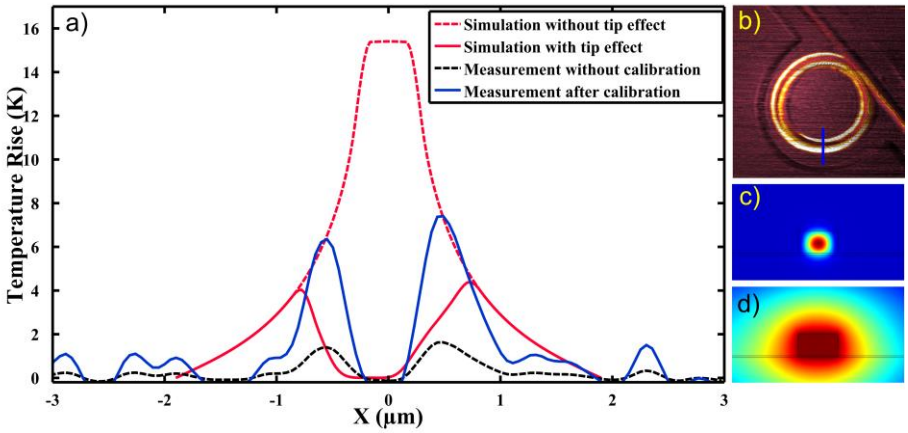

Fig. 6. (a) Simulation and measurement results of the temperature profile in a cross section of the ring waveguide. The dashed black line and the solid blue line represent measurement results before and after calibration, respectively. The dashed (solid) red line represents simulation results without (with) consideration of the tip effect. The simulation results were obtained for 113mW of optical power in the ring and 1% loss to heat. (b) The original thermal scan with the taken cross section marked in blue line. (c) 2D simulation showing a cross section of the optical intensity profile of the first TE mode (d) 2D simulation showing a cross section of the temperature distribution as a result of light absorption in the waveguide.

The analysis of our result clearly shows that a significant temperature rise occur in the MRR. With only 2mW of light propagating in the waveguide, a temperature rise of up to 10°C was observed. Given the thermo optic coefficient of silicon ($1.8\cdot10^{-4}$ K^{-1}) [32], and mode confinement of ~0.8, this temperature rise correspond to a shift in the wavelength of resonance of about 0.05%, i.e. ~0.8 nm. Obviously, such a large shift poses a stringent limitation on the applicability of nanoscale devices such as MRRs as active silicon photonic components such as modulators. The same order of shift in resonance wavelength was previously observed in active modulator device based on MRR with slightly different geometrical and doping parameters [33]. Different ways to compensate for the shift in resonance wavelength due to the effect of thermal heating were recently proposed and demonstrated, e.g. an active heat control by using thermal heaters [34], engineering the thermal resistance of MRR devices [33,35] and by using a multiple cavity coupled devices [36]. Nevertheless, further design effort is needed in order to reduce the effect of thermal heating. Specifically, the effect of thermal heating can be suppressed by using a thicker rib section. Given the excellent thermal conductivity of silicon, this rib section can be used for the purpose of heat removal.

4. Conclusion

Following the shrinkage in feature size of advanced nanophotonics devices, self-heating in photonic components is becoming a troublesome issue owing to the increasing optical power densities and the significant light absorption in the materials. Therefore, similar to electronics, nanoscale thermal characterization of photonic devices is important for understanding the underlying physics of self heating at the nanoscale as well as for the development of advance on chip photonic components and circuits. In this paper we demonstrated a direct measurement of self heating in a doped-silicon MRR, using thermocouple-based SThM scheme. The measurements present clear evidence of temperature rise following linear absorption in the MRR. The amount of temperature rise was evaluated using a separate calibration process, and it was found to be in reasonable agreement with the value predicted by the simulation. Taking into account the perturbation of the tip and performing a size dependent calibration process, we estimate the temperature rise to be in the order of 10°C for power levels of 2mW in the waveguide. Such a significant heating may jeopardize the role of

#197482 - $15.00 USD Received 10 Sep 2013; revised 3 Nov 2013; accepted 5 Nov 2013; published 18 Nov 2013
(C) 2013 OSA

miniaturized devices such as microring resonators in becoming a building block in active silicon photonic components. Clearly, future designs of such devices should optimize not only the optical and electrical properties of such devices, but also the aspect of efficient heat removal. Finally, while the SThM approach allows for direct thermal measurement with submicron resolution, there is a need to account for the effect of tip perturbation and also to perform calibration process which depends both on the probe and the sample dimensions, limiting the accuracy of the approach. Future effort should be devoted into developing automated pre-measurement procedures which take these effects into account.

Acknowledgments

The research was supported by the AFOSR. Mor Tzur acknowledges financial support from the Peter Brojde Center for Innovative Engineering and Computer Science. Ilya Goykhman and Boris Desiatov acknowledge the Eshkol fellowship from the ministry of science and technology. The devices were fabricated at the Center for Nanoscience and Nanotechnology, of the Hebrew University of Jerusalem.

#197482 - $15.00 USD Received 10 Sep 2013; revised 3 Nov 2013; accepted 5 Nov 2013; published 18 Nov 2013
(C) 2013 OSA

132.64.56.48 {ts '2020-07-31 14:08:01'}